PCCP

Using an aromatic linker to optimize charge-resonance states, photodimerization and reversibility in covalent anthracene dimers

Journal:	*Physical Chemistry Chemical Physics*
Manuscript ID	CP-ART-10-2024-004022.R1
Article Type:	Paper
Date Submitted by the Author:	24-Jan-2025
Complete List of Authors:	Lam, Kevin; UC Riverside, Department of Chemistry Dillon, Robert J.; US Army Combat Capabilities Development Command Army Research Laboratory; UC Riverside, Department of Chemistry Carreras, Abel; Multiverse Computing SL Nishiuchi, Tomohiko; Osaka University School of Science Graduate School of Science, Department of Chemistry Kubo, Takashi; Osaka University School of Science Graduate School of Science, Department of Chemistry Al-Kaysi, Rabih; King Saud bin Abdulaziz University for Health Sciences; King Abdullah International Medical Research Center Casanova, David; Donostia International Physics Center; Basque Foundation for Science Bardeen, Christopher; UC Riverside, Department of Chemistry

Using an aromatic linker to optimize charge-resonance states, photodimerization and reversibility in covalent anthracene dimers

Kevin Lam[(1)], Robert J. Dillon[(1)(2)], Abel C. Conill[(3)*],Tomohiko Nishiuchi[(4)], Takashi Kubo[(4)*], Rabih O. Al-Kaysi[(5)], David Casanova[(6)], Christopher J. Bardeen[(1)*]

[(1)]Department of Chemistry
University of California, Riverside
Riverside, CA 92521, USA

[(2)] U.S. Army Combat Capabilities Development Command, Army Research Laboratory
2800 Powder Mill Rd
Adelphi, MD 20783, USA

[(3)]Multiverse Computing, 20014 Donostia, Euskadi, Spain

[(4)]Department of Chemistry, Graduate
School of Science, Osaka University,
Toyonaka, Osaka, Japan

[(5)]College of Science and Health Professions-3124,
King Saud bin Abdulaziz University for Health Sciences, and King Abdullah International Medical Research Center (Nanomedicine), Ministry of National Guard Health Affairs, Riyadh 11426, (Kingdom of Saudi Arabia)

[(6)]Donostia International Physics Center (DIPC) 20018, Donostia, Euskadi, Spain
[‡]IKERBASQUE – Basque Foundation for Science, 48009, Bilbao, Euskadi, Spain

Abstract

The intramolecular [4+4] photodimerization of anthracene chromophores in covalent assemblies can be harnessed to create negative photochromic systems. This paper reports the characterization of the photophysical and photochemical properties of a new class of asymmetric phenyl-linked bis(anthracene) photochromes and compares their behavior with that of a previously studied symmetric ethylene-linked analog. Steady-state and femtosecond time-resolved spectroscopic experiments show that both types of bis(anthracenes) support a neutral bright state along with a

lower-energy charge resonance state. After photoexcitation, both states relax on sub-10 ps timescales, but with significantly different photodimerization quantum yields: 0.83 using 532 nm excitation of the charge-resonance state versus 0.46 for 400 nm excitation of the neutral bright state. The phenyl-linked bis(anthracene) derivatives exhibit superior thermal stability and reversibility due to a lower activation energy for dimer dissociation (94 kJ/mol versus 110 kJ/mol). Quantum chemical calculations reveal the structure of the neutral and charge-resonance excited states and can rationalize the higher photodimerization quantum yield of the latter. The phenyl linker enforces close alignment of the anthracene moieties, shifting the charge resonance state to lower energy and extending the wavelength range of the photochrome while also raising the energy of the photodimer ground state to enhance the backward reaction rate. The phenyl-linked bis(anthracenes) provide a promising system to harness the [4+4] photodimerization reaction with high quantum yield, room temperature reversibility, and cyclability.

Introduction

Photochromic molecules have a variety of applications, including sensing, biological imaging, information storage, and photomechanical actuation.[1] There are ongoing efforts to develop new classes of photochromes that rely on different photoisomerization reactions. Commonly used unimolecular reactions are the E-Z photoisomerization supported by azobenzenes[2, 3], hydrazone derivatives[4-6], and the diarylethene ring opening-closing reaction popularized by Irie and coworkers.[7] These molecules are usually classified as positive photochromes whose reactant and product absorption spectra have substantial overlap. The overlapping absorption spectra lead to two related problems. First, if the reaction can be reversed by photoisomerization of the product (P-type reversibility), then a photostationary state (PSS) will be established that prevents 100% conversion of the sample. Second, even in the absence of P-

type reversibility, the photoproduct absorption prevents the actinic light from reaching subsurface reactant molecules in optically thick samples. Often, both effects are present, and the establishment of an absorbing PSS on the front face of a sample prevents photons from ever reaching reactant molecules on the back side.

Negative photochromism offers a route to achieve 100% conversion of optically thick samples.[8] In negative photochromes, the product absorption is blue-shifted from the reactant absorption, so the actinic light can pass through to convert the layers behind it. There is no PSS present because the product cannot absorb the incoming photons. To achieve negative photochromism, the photoisomerization must disrupt conjugation within the reactant photochrome. Most unimolecular photoisomerizations, like the E-Z bond rotation, do not lead to a dramatic change in π-conjugation. Cycloaddition reactions provide a way to disrupt conjugation thanks to the conversion of sp^2 carbons to sp^3 carbons. This can be accomplished in a unimolecular reaction, as in the donor acceptor Stenhouse adduct class of photochromes that undergo a multistep cyclization to completely eliminate absorption in the visible region.[9, 10] Bimolecular reactions, like [2+2] and [4+4] photocycloadditions, provide another route to obtain negative photochromism.[11, 12] These photochemical reactions shift the product absorption well into the ultraviolet (UV) region and typically require either the application of deep UV light or a thermal reaction to restore conjugation. Thermally reversible (T-type) photochromes have applications in light-gating and photomechanical actuation[12-14], and the timescale of this reversibility is a key factor in such applications.

Intermolecular photocyclization reactions can be very efficient in crystals but tend to be slow in solution, where diffusive encounters between an excited molecule and a second molecule are required. To circumvent this problem, it is possible to use covalent linkers to tether

photoreactive chromophores together and enable intramolecular photodimerization. For example, a variety of linkers have been used to position a pair of anthracene moieties to undergo intramolecular [4+4] photodimerization (Scheme 1)[4, 15-26], and this reaction has been harnessed to make ion sensors.[16, 27, 28] Most of these bis(anthracene) compounds have been made with single or relatively flexible tethers that do not enforce close contact between the constituent anthracenes. To improve photodimerization quantum yields, workers have experimented with short-chain alkane tethers, with the most-well-studied being bi(anthracene-9,10-dimethylene) (**1**) and similar derivatives.[29-33] This molecule relies on symmetric ethylene linkers to connect the anthracenes and undergoes photodimerization with quantum yields approaching unity. It has been proposed as a candidate for photochemical solar energy storage[34], but its low solubility and thermal stability (see below) make such applications challenging.

Kubo and coworkers recently developed a synthetic pathway for making asymmetric bis(anthracene) derivatives, in which one of the ethyl linkers is replaced by a phenyl group. [35-37] This architecture confers additional rigidity to reduce conformational freedom, while also providing a convenient handle to attach other functional groups, for example alkoxy chains to improve solubility. (-H)mono-benzoannulated [2.2](9,10)anthracenophane (**2)** and (-OEt)mono-benzoannulated [2.2](9,10)anthracenophane (**3**) belong to this new class of bis(anthracene) photochromes, and we wanted to assess and compare their photophysical and photochemical properties to those of the more well-studied molecule **1** (Scheme 1). Steady-state and time-resolved spectroscopic methods are used to characterize their electronic structure and relaxation dynamics, while their temperature and solvent dependent reaction rates allow us to assess the reversibility of the photodimerization. Quantum chemical calculations provide a basis for the assignment of neutral and charge-resonance excited states, as well as a way to rationalize the

wavelength dependent quantum yield and trends in dimer dissociation. The phenyl linker enforces close alignment of the anthracene moieties, shifting the intermolecular charge resonance state to lower energy and extending the wavelength sensitivity of the photochrome. It also increases steric strain within the photodimer to enhance the thermal (T-type) reversibility. These changes allow the asymmetric bis(anthracene) derivatives to exhibit superior stability, solubility, and reversibility as compared to the symmetric bis(ethyl)anthracene. This study illustrates that it is possible to design covalent assemblies that harness interchromophore coupling to generate novel and useful properties in a negative photochromic system.

Experimental

Synthesis: The synthesis of bi(anthracene-9,10-dimethylene) (**1**) was accomplished following the method described by Golden[29] with slight modification (Supporting Information). In short, 9,10-bis(chloromethyl)anthracene and sodium iodide were slowly added to a mixture of excess sodium iodide in acetone and allowed to reflux under a blanket of argon gas for 24 hours. Subsequent purification and multiple recrystallization steps resulted in the formation of small orange crystals. The synthesis of (-H)mono-benzoannulated [2.2](9,10)anthracenophane (**2**) was performed as recently described.[36] The synthesis of (-OEt)mono-benzoannulated [2.2](9,10)anthracenophane (**3**) was achieved in a similar manner as **2** and is described in detail within the supporting information.

Steady-state spectroscopy: Solutions were prepared in a 1 cm path length quartz cuvette. Forward reaction rate measurements were performed using a Cary 60 UV/vis spectrophotometer. An AloneFire SV13 LED 365 nm flashlight and a diffused continuous wave 532 nm laser were

used as the excitation source for these experiments. To measure the reverse dissociation rates at various temperatures, a Cary 500 UV/vis spectrophotometer with a built-in heating block was used.

Ultrafast spectroscopy measurements: Transient absorption experiments were performed using a 1 kHz regeneratively amplified laser system (Coherent Libra). Experiments were conducted with either 400 nm or 470 nm photoexcitation. The 400 nm pump beam was produced via frequency doubling of the 800 nm laser fundamental in a BBO crystal, and the 470 nm pump was achieved by optical parametric amplification (Quantronix Palitra) of the fundamental to 1880 nm and subsequent frequency doubling performed twice in two BBO crystals. In both cases, residual laser beams (fundamental, signal, idler, etc.) were removed with selectively reflective optics. A supercontinuum probe was produced from another portion of the fundamental that was focused into a sapphire plate. The pump was modulated to 500 Hz via a mechanical chopper. A half-wave plate on the pump beamline was employed to set the relative polarization of pump and probe to magic angle. A 775 nm short-pass filter was used on the probe beamline to remove the majority of residual fundamental from the supercontinuum prior to reaching the sample, and an additional hot-mirror and KG5 color filter were positioned after the sample to optimize the signal into the detector (Ultrafast Systems). Samples in chloroform solvent were flowed through a quartz 1 mm pathlength cell using a peristaltic pump to ensure a fresh volume of sample for every laser pulse. Clean solvent was used to repeatedly flush the cell and tubing lines in between samples. The sample cell was positioned just before the focus of the pump beam. The sizes of the 400 and 470 nm pump beams at the sample position were measured by translation of a razorblade via a computer-controlled actuator. Neutral density filters were used to attenuate the power of the pump beam; the per pulse fluence of the 400 nm pump was 0.74 mJ/cm^2 , and the 470 nm pump was 0.20

mJ/cm^2. Results were chirp-corrected according to the cross-correlation of pump and probe measured by frequency-resolved optical gating experiments on pure chloroform. Chirp-correction and data analysis were performed with home built LabView software.

Electronic structure calculations. Molecular geometries have been optimized within the density functional theory (DFT) with the CAM-B3LYP exchange-correlation functional[38] and the cc-pVDZ. CAM-B3LYP employs a range-separated approach that combines short-range GGA exchange with long-range Hartree-Fock exchange. This balance improves the description of electronic excitations, especially in systems with significant charge-transfer character, which are of major relevance in the present study. A multitude of studies have shown that CAM-B3LYP provides reliable excitation energies for a variety of organic molecules, often outperforming traditional functionals that lack long-range correction.[39] Concretely, in a recent benchmarking study on the accuracy of DFT functionals for excited-state calculations[40], CAM-B3LYP was among the best-performing functionals, with average deviations of approximately 0.20 eV or slightly below, indicating its reliability in modeling excited states of organic chromophores. Dispersion interactions have been included by means of the D3 empirical correction with the Becke-Johnson (BJ) damping function.[41] Excited states have been obtained with the linear-response time-dependent DFT (TDDFT) within the Tamm-Dancoff approximation (TDA)[42] using the same energy functional and basis set. Excitation energies and oscillator strengths calculated with the cc-pVDZ and cc-pVTZ basis sets show only minor differences (Table S2). The convergence criterion for all Kohn-Sham self-consistent calculations was set to 10^{-8} a.u. For TDDFT/TDA calculations, energy convergence was achieved when the residual fell below 10^{-6} a.u. Two-electron integrals involving orbital pairs with overlaps smaller than 10^{-14} a.u. were neglected in all calculations. All these calculations were performed with the Q-Chem program.[43]

The character of electronic transition were quantified through the analysis of transition density matrices as implemented in the Theodore package.[44]

Results

1. Steady-State Spectroscopy and Reaction Kinetics

The synthesis of molecules **1-3** is described in detail in the Supporting Information and followed previous literature procedures.[29, 35, 36] We found that multiple recrystallization steps were required to isolate pure **1**. For samples that were not subject to rigorous purification, we found that exposure to 365 nm light led to the appearance of an anthracene-like peak that never completely disappeared, even after prolonged irradiation (Figure S11). The surviving peak resembled that of monomeric anthracene, and its amplitude varied according to the number of purification steps performed on the sample. The best explanation for these observations is that larger ring oligomers containing $n>2$ anthracene moieties were formed during the synthesis. These larger rings would prevent facile dimerization because the anthracenes along the circumference would no longer be cofacial.

The crystal structures of **1-3** show that they all adopt a cofacial arrangement[29, 36, 45] in which the anthracene rings are within the 4.1 Å distance required for photodimerization[46] (Figure S12). The close approach of the anthracene rings enables strong electronic interactions that affect the electronic state structure. These effects can be seen by examining the absorption spectrum of **1** (Figure 1). There is a high energy feature, peaked at 382 nm, that occurs in roughly the same location as monomeric anthracene. For the purposes of this paper, we associate this strongly absorbing high energy feature with a bright excited state denoted S_B. In **1**, this feature exhibits a distorted vibronic peak progression whose intensities do not follow the classic Huang-Rhys pattern

seen in anthracene.[47] The decreased 0-0 peak amplitude relative to the 0-1 and 0-2 peaks is suggestive of a strong excitonic interaction between the anthracene chromophores. The decrease in 0-0 intensity is characteristic of an H-type dimer[48], as expected based on the parallel transition dipole moments (TDMs) in the cofacial anthracene pair. At lower energies, a shoulder that extends past 500 nm can be seen. This low-energy feature has been assigned to an intramolecular excimer or charge transfer (CT) state by previous workers[31, 49], and here we denote it as the S_A state.

The phenyl-linked molecule **2** shares the same qualitative absorption features as **1**, but with several important differences, as shown in Figure 1. First, the lineshape of the high-energy S_B feature more closely resembles that of monomeric anthracene, with a dominant 0-0 peak and decreasing 0-1 and 0-2 peak intensities. The relative peak intensities are still distorted, with the 0-0/0-1 ratio slightly higher than seen for anthracene, but nothing like the large changes seen in **1**. Second, the S_B feature of **2** and **3** has about twice the absorption strength of **1**. Its peak absorption coefficient of 16000 $M^{-1}cm^{-1}$ is what is expected for a pair of independent anthracene molecules, each contributing a value of 8000 $M^{-1}cm^{-1}$. Third, the low-energy S_A feature for molecules **2** and **3** is shifted farther to the red while maintaining approximately the same absorption strength. The absorption spectrum of molecule **3** is almost indistinguishable from that of **2**, showing that addition of the alkoxy group *meta* to the linker groups has a negligible effect on the electronic state structure.

When solutions of **1-3** were exposed to either visible or UV light, the absorption at wavelengths greater than 300 nm rapidly disappeared. Examples of this absorption change are shown in Figure 2 for molecules **1** and **2**. The reaction rates in chloroform were measured for 365 nm and 532 nm irradiation. We used these rates, along with the measured intensities and absorption cross sections, to estimate photodimerization quantum yields (Table S1). At 365 nm,

we obtained quantum yield values of 0.47 ± 0.05 and 0.54 ± 0.07 for **2** and **3** respectively, close to the values in the range 0.25-0.45 reported previously for **1**[32, 50, 51] Interestingly, the photodimerization became significantly more efficient when the lower energy S_A feature was excited, rising to 0.83 ± 0.09 for **2** when 532 nm light was used. The increased quantum yield for longer wavelengths was again consistent with previous results for **1**.[51] Excitation of both the S_A and S_B states can lead to the photodimer product, but the wavelength dependent quantum yields indicate distinct pathways from each state.

The dissociation of the photodimer back into a pair of intact anthracenes is necessary for these molecules to function as T-type photochromes, and the differences between **1** and **2-3** became more pronounced when this reaction was examined. To determine the activation energy (E_{act}) for photodimer dissociation, the time-dependent recovery of the visible absorption was measured as a function of temperature. An exponential fit of this data yielded the rate for dimer dissociation back into a pair of anthracenes (k_{back}). The recovery data, along with the resulting Arrhenius plots, are shown in Figure 3 for molecules **1-3**. If we limit our analysis to the temperature range 25-55°C, we obtain E_{act} =94.3 ± 2.0 kJ/mole and A = 4×10^{12} s^{-1} for **2**, in good agreement with previous measurements over the same temperature range.[36] The addition of the ethoxy group resulted in almost identical values, E_{act} = 93.1 ± 3.2 kJ/mole and A = 3×10^{12} s^{-1} for **3**. For **1**, we found E_{act} = 110.1 ± 2.5 kJ/mole and A = 3×10^{13} s^{-1}. We note that **1**'s E_{act} value is higher than previously measured values that range from 93-100 kJ/mol.[32, 52, 53] We suspect that the different E_{act} values may arise from deviations from linear Arrhenius behavior at higher temperatures, 60-80°C, seen in Figure 3b. At higher temperatures, the rate does not increase as rapidly as predicted by the Arrhenius relation, leading to a roll-over of the points for smaller 1/T values. If all these points are included in a linear fit, the slope of the line will be smaller (and the

E_{act} value lower) than if a smaller temperature range is analyzed. This deviation from linearity suggests that the photodimer dissociation may not be a simple one-step process and could involve a pre-equilibrium formation of a reactive conformation.[54, 55] In any case, the lower E_{act} values for molecules **2**-**3** lead to room temperature photodimer dissociation times of a few hours versus weeks for **1**. This more rapid dissociation occurs even though **1** has a higher A prefactor value, most likely due to its greater flexibility. Note that untethered anthracene photodimers in solution, like those formed by anthracene and 9-methylanthracene, tend to have even higher E_{act} values on the order of 150 kJ/mole and much longer lifetimes.[56, 57] The lower E_{act} for **2** and **3** suggests that the inflexibility of the aromatic linker adds strain to the photodimer and lowers its stability, which enhances its thermal reversibility.

When **1** was held at elevated temperatures (90°C) for more than 10 minutes, it decomposed into a species whose absorption spectrum closely resembled that of monomeric anthracene (Figure S13). This species was not photochemically active. In contrast, **2** was highly stable and underwent the reversible photodimerization at all temperatures (Figure S14). The photochromism of molecules **2** and **3** was also highly fatigue-resistant: **2** could be cycled 100 times in solution without measurable loss of absorption (Figure S14).

2. Time-resolved Spectroscopy Measurements

The high photodimerization quantum yields and lack of fluorescence in the bis(anthracenes) suggest that the excited state reaction dynamics are quite rapid. Interestingly, we could not find a direct measurement of the [4+4] photodimerization rate starting from a well-defined geometry like a crystal or rigid dimer. We performed fs-TA experiments on molecules **1** and **2** in chloroform and observed similar excited state dynamics in both. Spectral snapshots of **1**

and **2** at various delays after the 400 nm pump pulse are shown in Figure 4a and 4c. A broad excited state absorption with peaks at 450 nm and 710 nm appears immediately after photoexcitation and decays to close to the baseline within 50 ps. In both molecules, the early decay at all wavelengths could be fit to a biexponential decay whose parameters are given in Table 1. The biexponential fits are overlaid with the single wavelength traces in Figure 4b and 4d, respectively. Both molecules show a rapid initial decay time constant τ_1 = 0.5-0.7 ps, with this contribution being larger for **1**. The slower component has τ_2 = 2.3 ps for **1** and τ_2 = 8.1 ps for **2**.

The 400 nm excitation wavelength overlaps both $S_0 \rightarrow S_A$ and $S_0 \rightarrow S_B$ transitions. To clarify the origin of the two time components, we tuned the excitation wavelength 470 nm to selectively excite the S_A state. Under these conditions, the excited-state absorption of molecule **2** exhibited a single exponential decay with a time constant of 8.1 ps, identical to the τ_2 component measured using 400 nm excitation (Figure 5a). This allowed us to assign τ_2 to the decay of S_A and the fast component τ_1 to the decay of S_B. It is possible that some component of the τ_1 relaxation involves transfer of population from S_B to S_A, but the lower quantum yield value for 400 nm excitation suggests that at least some of the S_B population undergoes internal conversion directly back to the ground state.

At probe delays >100 ps, the TA spectrum after 400 nm excitation ceased to evolve but did not quite return to the baseline (Figure 5b). Two weak features could be discerned above the noise level, with $\Delta A/A$ values at <5% of the early time excited state absorption signal. For λ<500 nm, there is a negative feature corresponding to a long-lived ground state bleach. This feature is expected because the photodimerization removes ground state molecules permanently from the probe volume. The long-lived positive feature peaked at around 700 nm is more difficult to explain. It is present in both **1** and **2** at the same relative size, so it is unlikely to be due to an

impurity. We suspect that a small fraction of the CT state population undergoes intersystem crossing to a long-lived triplet excimer state that gives rise to this feature. The anthracene monomer triplet has a strong absorption feature at around 450 nm[58] that is not observed in the data, but both singlet and triplet aromatic excimers tend to have broad, redshifted absorption features similar to those in Figure 5b.[59, 60] Alternatively, this feature could be due to a nonreactive conformation of the dimers, but it would be surprising if such a conformation was present in similar populations for both **1** and **2**.

3. Computational Analysis of Electronic Structure

The interpretation the spectroscopic results in the previous sections can be facilitated by a more detailed understanding of the low-lying excited states of the bis(anthracenes). Using the CAM-B3LYP-D3 energy functional, we found that the ground state optimized geometries of compounds **1** and **2** closely match their crystal structures, exhibiting a nearly coplanar alignment between the two anthracene backbones (Figure 6). In compound **1**, the double ethylene linkage permits a slip-stacked configuration, facilitating favorable π-π staggered stacking interactions between the two aromatic units.[61] Conversely, in compound **2** the presence of the phenyl tether compels the anthracene units to adopt a more closely eclipsed disposition.

The first question involves the origin of the low-energy feature in the absorption spectra around 500 nm. Excited state calculations show that the transition to the lowest excited singlet state (S_A) mainly corresponds to the one electron promotion from the highest occupied molecular orbital (HOMO) to the lowest unoccupied molecular orbital (LUMO). Both frontier MOs are symmetrically delocalized over the two anthracenes, obtained as the combination of the monomeric counterparts and exhibiting out-of-phase and in-phase π-π interactions, respectively

(Figure 7). From the set of singlet states generated by the calculations, we assign S_A to the calculated S_1 state for both **1** and **2**, and S_B to S_3 and S_4 for **1** and **2** respectively. Computed oscillator strengths for the transition to S_1 are quite small in both molecules, consistent with the experimentally observed weak absorption band at longer wavelengths. Notably, the calculated oscillator strength for S_1 in molecule **1** is zero, indicating an optically inactive transition. However, it is important to note that these calculations were performed on a single frozen geometry optimized for the ground state. In reality, thermal fluctuations at room temperature could enable weak transitions to S_1. The excitation energy to S_A in **2** is about 0.2 eV lower than in **1** (Table S2), in agreement with the redshift observed in the absorption spectra of **2**-**3** with respect to **1**. The more pronounced redshift of S_A in **2** emerges from ground state structural differences, with the near eclipsed conformation in **2** stabilizing the LUMO due to more efficient in-phase π-π overlap. Analysis of the nature of the transition identifies S_A in both **1** and **2** as a linear combination of equally weighted local excitations on each anthracene unit and symmetric inter-anthracene CT contributions (from one monomer to the other and vice versa), i.e., charge resonance (CR), with an overall ~45% CR character (Table 2).

The $S_0 \rightarrow S_A$ transition involves the removal of an electron from an orbital with inter-anthracene antibonding-like interaction (HOMO) to an orbital with bonding character (LUMO), that is, an increase of the π-bond order. Hence, energy relaxation on the S_A potential energy surface (PES) aims to enhance the π-overlap. As a result, optimal structures of **1** and **2** on the S_A state (Figure 6) present an eclipsed arrangement of the two anthracenes with considerably reduced C-C distances (approximately 0.2 Å shorter than in S_0). This structural change involves large reorganization energies of 1.12 and 0.98 eV for **1** and **2**, respectively. The composition of the relaxed S_A state remains similar to that of the initially excited S_A state in the ground state geometry,

with a slight increase of the CR character (~48 %). Considering the strong interchromophore interaction, emission redshift, and composition of the transition, we label S_A as an intramolecular excimer, in agreement with previous assignments.[31, 49] Notably, the short C-C distances at the pro-dimerization atomic positions, 2.57 Å (**1**) and 2.59 Å (**2**), suggest that the relaxed excimer state is a potential intermediate facilitating the photoinduced molecular dimerization.

The high energy absorption band at ~382 nm is characterized by the transition to a singlet bright state (S_B), obtained as the HOMO-1→LUMO and HOMO→LUMO+1 contributions (Figure 7). In contrast to S_A, the S_B state almost entirely corresponds to the combination of local excitations on each anthracene fragment (maximum 5% CT state participation, Table 2), with parallel alignment of the local TDMs along the short anthracene molecular axis. The strong excitonic interaction between the anthracene chromophores is confirmed by the classical dipole-dipole approach, with point-dipole couplings in the order of 290 meV. This value decreases to 70 meV when a multi-dipole approach is used. There was no significant difference in the calculated excitonic coupling for molecules **1** and **2**.

Geometrical relaxation on the S_B PES does not involve major structural changes, e. g., the distance between anthracene rings changes by less than 0.02 Å with respect to the ground state geometry. The associated reorganization energy for S_B is also much smaller than in the excimer formation (0.24 eV in **1** and **2**). These findings elucidate why excitation at 365 nm leads to less efficient molecular dimerization. Excitation to the S_A state primes an intramolecular excimer state conducive to photodimerization, whereas populating the bright state leads to a relaxed state that is basically a neutral anthracene unit subject to Coulombic coupling with its neighbors but with no obvious driving force for bond formation between the two anthracene units.

Electronic structure calculations confirm that the presence of the phenyl linker in **2** reduces the stability of the photodimer (**2'**) relative to the reactant form. With respect to the reactant ground state, the photodimer form is 20.5 kJ/mol higher in **1** and 38.9 kJ/mol higher in **2**. If we assume that the transition state energies are similar for **1** and **2**, then the ground state of photodimer **2'** is about 18 kJ/mol closer to the transition state than that of **1'**. This energy difference is very close to the 16 kJ/mol energy difference in E_{act} values measured for these two molecules. The more rapid reversibility of the phenyl linker can be attributed almost entirely to the destabilization of the photodimer due to increased ring strain by the phenyl group that shortens one of the sides of the cyclobutane ring. This trend is consistent with calculations that indicate that the activation barrier for cyclobutane ring opening can be reduced by 50% or more by the presence of the aromatic ring on one of the arms.[62, 63] To characterize the increased ring strain in **2'**, we define the ring deformation function ϕ as the sum of the in-plane displacements of the atoms in the cyclobutane ring for each normal mode:

$$\phi(\omega) = \sum_{k}^{3N-6} \sum_{i=1}^{N_R} d_{ik}(\omega_k) \quad (1)$$

where N is the total number of atoms, N_R are the number of atoms in the ring, k runs over the molecular vibrational modes with ω_k frequency, and $d_{ik}(\omega_k)$ is the atomic in-plane displacement of atom i in the k-mode. Ring deformation functions obtained for photodimers **1'** and **2'** within the 700-1600 cm^{-1} region are shown in Figure 8. Comparison of the two profiles indicate that ring distortions in **2'** have a larger coupling to the high frequency C-C stretching modes (1300-1600 cm^{-1} region). The C-C stretching modes reflect motions that lead to bond breaking and dissociation, so this analysis suggests that the cyclobutane ring in **2'** is under more tension than that in **1'**.

Discussion

The level diagram in Figure 9 outlines two major changes in the bis(anthracene) photophysics that result from the use of a rigid phenyl linker to attach the anthracenes. First, it enforces more complete overlap of the conjugated rings in the ground state geometry, shifting the reactive S_A state to lower energies and increasing its separation from the S_B state. Fortunately, this change in S_A does not decrease the efficiency of the forward dimerization with respect to molecule **1**. Second, the phenyl linker raises the energy of the photodimer ground state, which lowers the activation energy for dissociation and improves thermal reversibility. From a practical perspective, the phenyl linker also serves to avoid the presence of oligomeric impurities seen for **1**, as well as the decomposition seen for **1** at higher temperatures. Lastly, the phenyl ring provides a convenient site for the attachment of chemical substituents to improve crystal packing or solubility.

While our work has provided a foundation for the further study of this class of molecules, there remain some open questions. One concerns the large change in the S_B absorption lineshape in going from **1** to **2**-**3**. Our calculations indicate a similar excitonic coupling for all three molecules, but the large change in absorption lineshape and intensity suggests that there is a significant change in the anthracene-anthracene interaction. It is possible that the flexibility of the ethylene linkers enables other conformations that have different excitonic coupling values than that of the crystal structure conformation. Temperature dependent absorption measurements of **1** in crystal form provide some support for this idea.[64] If **1**'s conformational freedom leads to large variations in excitonic coupling, that points to another advantage to using the more rigid phenyl linker.

A second issue concerns the wavelength-dependent quantum yield for the photodimerization. In all three molecules, the S_A excimer state has greater reactivity than the S_B state and its relaxed geometry points to its central role in the photodimerization. In acccordance with Kasha's Rule, one might expect the S_B state to relax into the S_A state before any dimerization or internal conversion to S_0 could occur, leading to no wavelength dependence of the quantum yield. It seems that the S_A and S_B states of bis(anthracene) support relaxation pathways that operate independently of each other. This phenomenon has been observed in other photochemical systems[65], notably azobenzene[66], and it originates from competing excited state relaxation processes. Several previous studies of anthracene photodimerization, including **1,** have suggested the role of a biradical intermediate in the photodimerization[32, 50, 67, 68], and it is possible that the role of this intermediate may depend on whether the S_A or S_B state is populated. The presence of such an intermediate in the dimer dissociation might also help explain the nonlinear behavior of the Arrhenius plots of the reverse reaction. Overall, the phenyl-linked molecules provide an opportunity to explore the electronic nature of the [4+4] photocycloaddition reaction in systems with structurally well-defined geometries. A full characterization of the excited state dynamics of this bichromophore system is reserved for future studies.

Conclusions

In this paper we have characterized a new class of phenyl-linked bis(anthracenes) that can function as negative photochromes. From a practical standpoint, the phenyl linker provides extra rigidity, thermal stability, and a location for the attachment of solubilizing groups. From an electronic structure standpoint, it shifts the reactive CR state to lower energy while raising the energy of the photodimer ground state, making it easier to access the forward photochemistry while

enhancing the backward reaction rate. While our theoretical calculations provide some qualitative rationales for the different quantum yields from the S_A and S_B states, further work in this area is clearly needed. The phenyl-linked bis(anthracenes) open up a practical route to harnessing the anthracene [4+4] photodimerization reaction in a photochromic assembly that combines high quantum yield, reversibility, fatigue resistance, and solubility. Further development of this class of molecules by modifying the linker and/or expanding the aromatic partners beyond anthracene should make it possible to develop a broad class of negative photochromic molecules that exhibit photochemically active, low energy charge-resonance states. This class of molecules provides a good example of how assembling multiple conjugated units in a controlled architecture can generate intermolecular electronic states that support novel optical properties and reactivity.

Acknowledgements

This work was supported by the Office of Naval Research through grant N00014-24-1-2358 (C.J.B.) and the King Abdullah International Medical Research Center (KSAU-HS/KAIMRC) through grant NRC21R25003 (R.O.K.). R.J.D. acknowledges Cooperative Research and Development Agreement ARL CRADA-15-033-00 facilitating collaboration between UCR and ARL. A. C. C. and D. C. thank the Spanish Ministry of Science and Innovation (projects MICINN/FEDER PID2022-136231NB-I00 and RED2022-134939-T) and acknowledge the technical and human support provided by DIPC Computer Center. This work was also supported by JSPS KAKENHI Grant-in-Aid for Scientific Research (C) JP20K05475 (T. N.), Scientific Research (B) 24K01454 (T. N.), and Transformative Research Areas (A) JP20H05865 (T.K.)

References

1. M. Irie, Y. Yokoyama and T. Seki, eds., *New Frontiers in Photochromism*, Springer, Tokyo, 2013.
2. C. J. Barrett, J.-I. Mamiya, K. G. Yager and T. Ikeda, *Soft Matter*, 2007, **3**, 1249-1261. **doi**: 10.1039/b705619b
3. H. M. D. Bandara and S. C. Burdette, *Chem. Soc. Rev.*, 2012, **41**, 1809-1825. **doi**: 10.1039/C1CS15179G
4. J. Manchester, D. M. Bassani, J.-L. H. A. Duprey, L. Giordano, J. S. Vyle, Z.-y. Zhao and J. H. R. Tucker, *J. Am. Chem. Soc.*, 2012, **134**, 10791–10794. **doi**: 10.1021/ja304205m
5. X. Su and I. Aprahamian, *Chem. Soc. Rev.*, 2014, **43**, 1963-1981. **doi**: 10.1039/C3CS60385G
6. D. J. v. Dijken, P. Kovaříček, S. P. Ihrig and S. Hecht, *J. Am. Chem. Soc.*, 2015, **137**, 14982–14991. **doi**: 10.1021/jacs.5b09519
7. M. Irie, T. Fukaminato, K. Matsuda and S. Kobatake, *Chem. Rev.*, 2014, **114**, 12174–12277.
8. S. Aiken, R. J. L. Edgar, C. D. Gabbutt, B. M. Heron and P. A. Hobson, *Dyes Pigm.*, 2018, **149**, 92-121. **doi**: 10.1016/j.dyepig.2017.09.057
9. S. Helmy, S. Oh, F. A. Leibfarth, C. J. Hawker and J. R. d. Alaniz, *J. Org. Chem.*, 2014, **79**, 11316–11329. **doi**: 10.1021/jo502206g
10. M. Clerc, S. Sandlass, O. Rifaie-Graham, J. A. Peterson, N. Bruns, J. R. d. Alaniz and L. F. Boesel, *Chem. Soc. Rev.*, 2023, **52**, 8245-8294. **doi**: 10.1039/D3CS00508A
11. W. J. Tomlinson, E. A. Chandross, R. L. Fork, C. A. Pryde and A. A. Lamola, *Appl. Opt.*, 1972, **11**, 533-548. **doi**: 10.1364/AO.11.000533
12. H. Dürr and H. Bouas-Laurent, eds., *Photochromism: Molecules and Systems*, Elsevier Science, Amsterdam, Netherlands, 2003.
13. S. Kobatake and Y. Terakawa, *Chem. Commun.*, 2007, DOI: 10.1039/B700177K, 1698-1700. **doi**: 10.1039/B700177K
14. L. Zhu, R. O. Al-Kaysi and C. J. Bardeen, *Angew. Chem. Int. Ed.*, 2016, **55**, 7073-7076. **doi**: 10.1002/anie.201511444
15. F. C. D. Schryver, N. Boens, J. Huybrechts, J. Daemen and M. D. Brackelaire, *Pure Appl. Chem.*, 1977, **49**, 237-247. **doi**: 10.1351/pac197749030237
16. I. Yamashita, M. Fujii, T. Kaneda, S. Misumi and T. Otsubo, *Tet. Lett.*, 1980, **21**, 541-544. **doi**: 10.1016/S0040-4039(01)85550-7
17. M. Daney, C. Vanucci, J.-P. Desvergne, A. Casterllan and H. Bouas-Laurent, *Tet. Lett.*, 1985, **26**, 1505-1508. **doi**: 10.1016/S0040-4039(00)98537-X
18. M. Usui, Y. Shindo, T. Nishiwaki, K. Anda and M. Hida, *Chem. Lett.*, 1990, DOI: 10.1246/cl.1990.419, 419-422. **doi**: 10.1246/cl.1990.419
19. J.-P. Desvergne, F. Fages, H. Bouas-Laurent and P. Marsau, *Pure Appl. Chem.*, 1992, **64**, 1231-1238. **doi**: 10.1351/pac199264091231
20. W. Rettig, B. Paeplow, H. Herbst, K. Müllen, J.-P. Desvergne and H. Bouas-Laurent, *New J. Chem.*, 1999, **23**, 453-460. **doi**: 10.1039/A809363F
21. H. Okamoto, M. Yamaji and K. Satakea, *Synlett*, 2008, DOI: 10.1055/s-2008-1078574, 1931–1945. **doi**: 10.1055/s-2008-1078574
22. Y. Oguma, M. Yamamoto, Y. Sunatsuki, H. Ota, M. Yamaji and H. Okamoto, *Photochem. Photobiol. Sci.*, 2024, **23**, 1509–1519. **doi**: 10.1007/s43630-024-00610-w

23. P. R. Christensen, B. O. Patrick, É. Caron and M. O. Wolf, *Angew. Chem. Int. Ed.*, 2013, **52**, 12946-12950. **doi**: 10.1002/anie.201306236
24. C. D. Cruz, J. Yuan, C. Climent, N. T. Tierce, P. R. Christensen, E. L. Chronister, D. Casanova, M. O. Wolf and C. J. Bardeen, *Chem. Sci.*, 2019, **10**, 7561–7573. **doi**: 10.1039/c8sc05598j
25. C.-K. Liang, J.-P. Desvergne and D. M. Bassani, *Photochem. Photobiol. Sci.*, 2014, **13**, 316–323. **doi**: 10.1039/c3pp50322d
26. A. Garci, Y. Beldjoudi, M. S. Kodaimati, J. E. Hornick, M. T. Nguyen, M. M. Cetin, C. L. Stern, I. Roy, E. A. Weiss and J. F. Stoddart, *J. Am. Chem. Soc.*, 2020, **142**, 7956−7967. **doi**: 10.1021/jacs.0c02128
27. J.-P. Desvergne and H. Bouas-Laurent, *J. Chem. Soc., Chem. Commun.*, 1978, DOI: 10.1039/C39780000403, 403-404. **doi**: 10.1039/C39780000403
28. H. Bouas-Laurent, A. Castellan and J.-P. Desvergne, *Pure Appl. Chem.*, 1980, **52**, 2633-2648. **doi**: 10.1351/pac198052122633
29. J. H. Golden, *J. Chem. Soc.*, 1961, DOI: 10.1039/JR9610003741, 3741-3748. **doi**: 10.1039/JR9610003741
30. T. Hayashi, N. Mataga, Y. Sakata, S. Misumi, M. Morita and J. Tanaka, *J. Am. Chem. Soc.*, 1976, **98**, 5910–5913. **doi**: 10.1021/ja00435a027
31. M. Morita, T. Kishi, M. Tanaka, J. Tanaka, J. Ferguson, Y. Sakata, S. Misumi, T. Hayashi and N. Mataga, *Bull. Chem. Soc. Japan*, 1978, **51**, 3449–3457. **doi**: 10.1246/bcsj.51.3449
32. W. R. Bergmark, G. J. II, T. E. Reinhardt and A. M. Halpern, *J. Am. Chem. Soc.*, 1978, **100**, 6665–6673. **doi**: 10.1021/ja00489a018
33. A. Dunand, J. Ferguson, M. Puza and G. B. Robertson, *J. Am. Chem. Soc.*, 1980, **102**, 3524–3530. **doi**: 10.1021/ja00530a036
34. G. J. II, T. E. Reinhardt and W. R. Bergmark, *Solar En.*, 1978, **20**, 241-248. **doi**: 10.1016/0038-092X(78)90103-2
35. T. Nishiuchi, S.-y. Uno, Y. Hirao and T. Kubo, *J. Org. Chem.*, 2016, **81**, 2106−2112. **doi**: 10.1021/acs.joc.6b00134
36. T. Nishiuchi, K. Kisaka and T. Kubo, *Angew. Chem. Int. Ed.*, 2021, **60**, 5400–5406. **doi**: 10.1002/anie.202013349
37. T. Nishiuchi, S. Takeuchi, Y. Makihara, R. Kimura, S. Saito, H. Sato and T. Kubo, *Bull. Chem. Soc. Japan*, 2022, **95**, 1591-1599. **doi**: 10.1246/bcsj.20220257
38. T. Yanai, D. P. Tew and N. C. Handy, *Chem. Phys. Lett.*, 2004, **393**, 51-57. **doi**: 10.1016/j.cplett.2004.06.011
39. P.-F. Loos, M. Comin, X. Blase and D. Jacquemin, *J. Chem. Theory Comput.*, 2021, **17**, 3666-3686. **doi**: 10.1021/acs.jctc.1c00226
40. I. Knysh, F. Lipparini, A. Blondel, I. Duchemin, X. Blase, P.-F. Loos and D. Jacquemin, *J. Chem. Theory Comput.*, 2024, **20**, 8152-8174. **doi**: 10.1021/acs.jctc.4c00906
41. S. Grimme, S. Ehrlich and L. Goerigk, *J. Comput. Chem.*, 2011, **32**, 1456-1465. **doi**: 10.1002/jcc.21759
42. S. Hirata and M. Head-Gordon, *Chem. Phys. Lett.*, 1999, **314**, 291-299. **doi**: 10.1016/S0009-2614(99)01149-5
43. E. Epifanovsky, A. T. B. Gilbert, X. Feng, J. Lee, Y. Mao, N. Mardirossian, P. Pokhilko, A. F. White, M. P. Coons, A. L. Dempwolff, Z. Gan, D. Hait, P. R. Horn, L. D. Jacobson, I. Kaliman, J. Kussmann, A. W. Lange, K. U. Lao, D. S. Levine, J. Liu, S. C. McKenzie, A. F. Morrison, K. D. Nanda, F. Plasser, D. R. Rehn, M. L. Vidal, Z.-Q. You, Y. Zhu, B.

Alam, B. J. Albrecht, A. Aldossary, E. Alguire, J. H. Andersen, V. Athavale, D. Barton, K. Begam, A. Behn, N. Bellonzi, Y. A. Bernard, E. J. Berquist, H. G. A. Burton, A. Carreras, K. Carter-Fenk, R. Chakraborty, A. D. Chien, K. D. Closser, V. Cofer-Shabica, S. Dasgupta, M. d. Wergifosse, J. Deng, M. Diedenhofen, H. Do, S. Ehlert, P.-T. Fang, S. Fatehi, Q. Feng, T. Friedhoff, J. Gayvert, Q. Ge, G. Gidofalvi, M. Goldey, J. Gomes, C. E. González-Espinoza, S. Gulania, A. O. Gunina, M. W. D. Hanson-Heine, P. H. P. Harbach, A. Hauser, M. F. Herbst, M. H. Vera, M. Hodecker, Z. C. Holden, S. Houck, X. Huang, K. Hui, B. C. Huynh, M. Ivanov, Á. Jász, H. Ji, H. Jiang, B. Kaduk, S. Kähler, K. Khistyaev, J. Kim, G. Kis, P. Klunzinger, Z. Koczor-Benda, J. H. Koh, D. Kosenkov, L. Koulias, T. Kowalczyk, C. M. Krauter, K. Kue, A. Kunitsa, T. Kus, I. Ladjánszki, A. Landau, K. V. Lawler, D. Lefrancois, S. Lehtola, R. R. Li, Y.-P. Li, J. Liang, M. Liebenthal, H.-H. Lin, Y.-S. Lin, F. Liu, K.-Y. Liu, M. Loipersberger, A. Luenser, A. Manjanath, P. Manohar, E. Mansoor, S. F. Manzer, S.-P. Mao, A. V. Marenich, T. Markovich, S. Mason, S. A. Maurer, P. F. McLaughlin, M. F. S. J. Menger, J.-M. Mewes, S. A. Mewes, P. Morgante, J. W. Mullinax, K. J. Oosterbaan, G. Paran, A. C. Paul, S. K. Paul, F. Pavošević, Z. Pei, S. Prager, E. I. Proynov, Á. Rák, E. Ramos-Cordoba, B. Rana, A. E. R. A. Rettig, R. M. Richard, F. Rob, E. Rossomme, T. Scheele, M. Scheurer, M. Schneider, N. Sergueev, S. M. Sharada, W. Skomorowski, D. W. Small, C. J. Stein, Y.-C. Su, E. J. Sundstrom, Z. Tao, J. Thirman, G. J. Tornai, T. Tsuchimochi, N. M. Tubman, S. P. Veccham, O. Vydrov, J. Wenzel, J. Witte, A. Yamada, K. Yao, S. Yeganeh, S. R. Yost, A. Zech, I. Y. Zhang, X. Zhang, Y. Zhang, D. Zuev, A. Aspuru-Guzik, A. T. Bell, N. A. Besley, K. B. Bravaya, B. R. Brooks, D. Casanova, J.-D. Chai, S. Coriani, C. J. Cramer, G. Cserey, I. A. Eugene DePrince, J. Robert A. DiStasio, A. Dreuw, B. D. Dunietz, T. R. Furlani, I. William A. Goddard, S. Hammes-Schiffer, T. Head-Gordon, W. J. Hehre, C.-P. Hsu, T.-C. Jagau, Y. Jung, A. Klamt, J. Kong, D. S. Lambrecht, W. Liang, N. J. Mayhall, C. W. McCurdy, J. B. Neaton, C. Ochsenfeld, J. A. Parkhill, R. Peverati, V. A. Rassolov, Y. Shao, L. V. Slipchenko, T. Stauch, R. P. Steele, J. E. Subotnik, A. J. W. Thom, A. Tkatchenko, D. G. Truhlar, T. V. Voorhis, T. A. Wesolowski, K. B. Whaley, I. H. Lee Woodcock, P. M. Zimmerman, S. Faraji, P. M. W. Gill, M. Head-Gordon, J. M. Herbert and A. I. Krylov, *J. Chem. Phys.*, 2021, **155**, 084801. **doi**: 10.1063/5.0055522

44. F. Plasser, *J. Chem. Phys.*, 2020, **152**, 084108. **doi**: 10.1063/1.5143076
45. J. Bakowicz and I. Turowska-Tyrk, *Crystals*, 2020, **10**, 1031. **doi**: 10.3390/cryst10111031
46. V. Ramamurthy and K. Venkatesan, *Chem. Rev.*, 1987, **87**, 433–481. **doi**: 10.1021/cr00078a009
47. T.-S. Ahn, A. M. Müller, R. O. Al-Kaysi, F. C. Spano, J. E. Norton, D. Beljonne, J.-L. Brédas and C. J. Bardeen, *J. Chem. Phys.*, 2008, **128**, 054505. **doi**: 10.1063/1.2822310
48. F. C. Spano, *Acc. Chem. Res.*, 2010, **43**, 429–439. **doi**: 10.1021/ar900233v
49. J. Ferguson, *Chem. Rev.*, 1986, **86**, 957–982. **doi**: 10.1021/cr00076a001
50. G. Kaupp, *Angew. Chem. Int. Ed.*, 1972, **11**, 313-314. **doi**: 10.1002/anie.197203131
51. H. Shizuka, Y. Ishii, M. Hoshino and T. Morita, *J. Phys. Chem.*, 1976, **80**, 30–32. **doi**: 10.1021/j100542a006
52. A. W. H. Mau, *J. Chem. Soc., Faraday Trans. 1*, 1978, **74**, 603-612. **doi**: 10.1039/F19787400603
53. S. R. Jezowski, L. Zhu, Y. Wang, A. P. Rice, G. W. Scott, C. J. Bardeen and E. L. Chronister, *J. Am. Chem. Soc.*, 2012, **134**, 7459-7466. **doi**: 10.1021/ja300424h
54. M. H. Han, *J. Theor. Biol.*, 1972, **35**, 543-568. **doi**: 10.1016/0022-5193(72)90150-6

55. J. R. Silvius and R. N. McElhaney, *J. Theor. Biol.*, 1981, **88**, 135-152. **doi**: 10.1016/0022-5193(81)90332-5
56. H. Bouas-Laurent, A. Castellan, J.-P. Desvergne and R. Lapouyade, *Chem. Soc. Rev.*, 2001, **30**, 248-263. **doi**: 10.1039/B006013P
57. J. Brancart, J. V. Damme, F. D. Prez and G. V. Assche, *Phys. Chem. Chem. Phys.*, 2021, **23**, 2252-2263. **doi**: 10.1039/d0cp05953f
58. I. Carmichael and G. L. Hug, *J. Phys. Chem. Ref. Data*, 1986, **15**, 1-250. **doi**: 10.1063/1.555770
59. R. Katoh, E. Katoh, N. Nakashima, M. Yuuki and M. Kotani, *J. Phys. Chem. A*, 1997, **101**, 7725–7728. **doi**: 10.1021/jp964075u
60. M. Yamaji, H. Tsukada, J. Nishimura, H. Shizuka and S. Tobita, *Chem. Phys. Lett.*, 2002, **357**, 137-142. **doi**: 10.1016/S0009-2614(02)00470-0
61. C. R. Martinez and B. L. Iverson, *Chem. Sci.*, 2012, **3**, 2191-2201. **doi**: 10.1039/C2SC20045G
62. B. Sirjean, P. A. Glaude, M. F. Ruiz-Lopez and R. Fournet, *J. Phys. Chem. A*, 2006, **110**, 12693–12704. **doi**: 10.1021/jp0651081
63. Z. Yuan, Q. Sun, J. Xiao, P. Zhang, K. S. Levchenko, D. Y. Demin and W. Fu, *Chin. J. Chem.*, 2023, **41**, 3238-3244. **doi**: 10.1002/cjoc.202300311
64. J. Ferguson, M. Morita and M. Puza, *Chem. Phys. Lett.*, 1977, **49**, 265-268. **doi**: 10.1016/0009-2614(77)80583-6
65. A. P. Demchenko, V. I. Tomin and P.-T. Chou, *Chem. Rev.*, 2017, **117**, 13353–13381. **doi**: 10.1021/acs.chemrev.7b00110
66. J. K. Yu, C. Bannwarth, R. Liang, E. G. Hohenstein and T. J. Martíne, *J. Am. Chem. Soc.*, 2020, **142**, 20680–20690. **doi**: 10.1021/jacs.0c09056
67. F. D. Greene, S. L. Misrock and J. R. W. Jr., *J. Am. Chem. Soc.*, 1955, **77**, 3852-3855. **doi**: 10.1021/ja01619a051
68. J. Michl, *Photochem. Photobiol.*, 1977, **25**, 141-154. **doi**: 10.1111/j.1751-1097.1977.tb07436.x

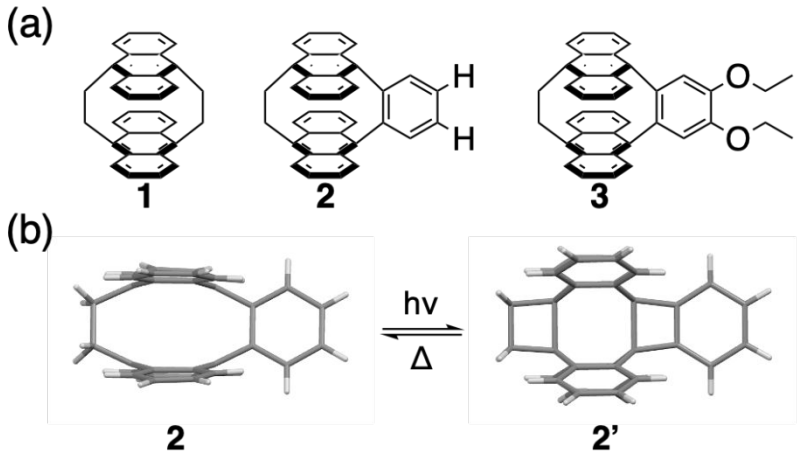

Scheme 1. (a) Chemical structures of the anthracene derivatives investigated in this paper: bi(anthracene-9,10-dimethylene) (**1**), (-H)mono-benzoannulated [2.2](9,10)anthracenophane (**2**) and (-OEt)mono-benzoannulated [2.2](9,10)anthracenophane (**3**). (b) [4+4] cycloaddition reaction scheme of **2**.

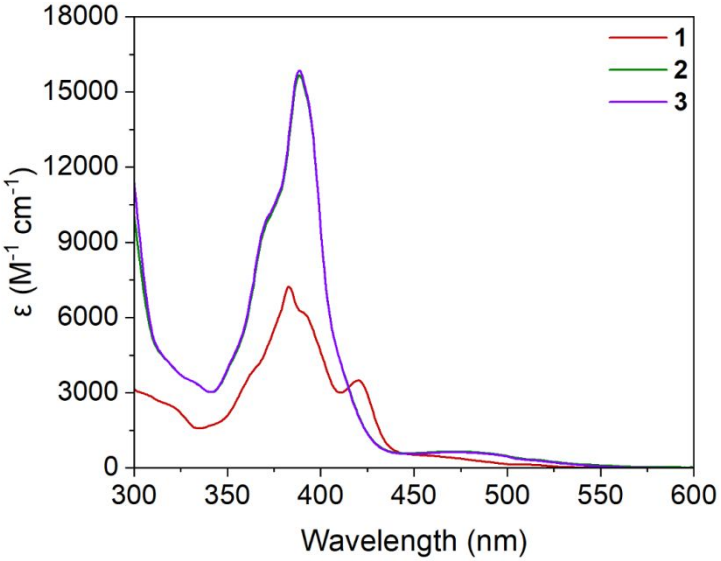

Figure 1. Steady-state UV/vis absorption spectra of **1-3** in chloroform. All sample concentrations were 3 x 10^{-5} M.

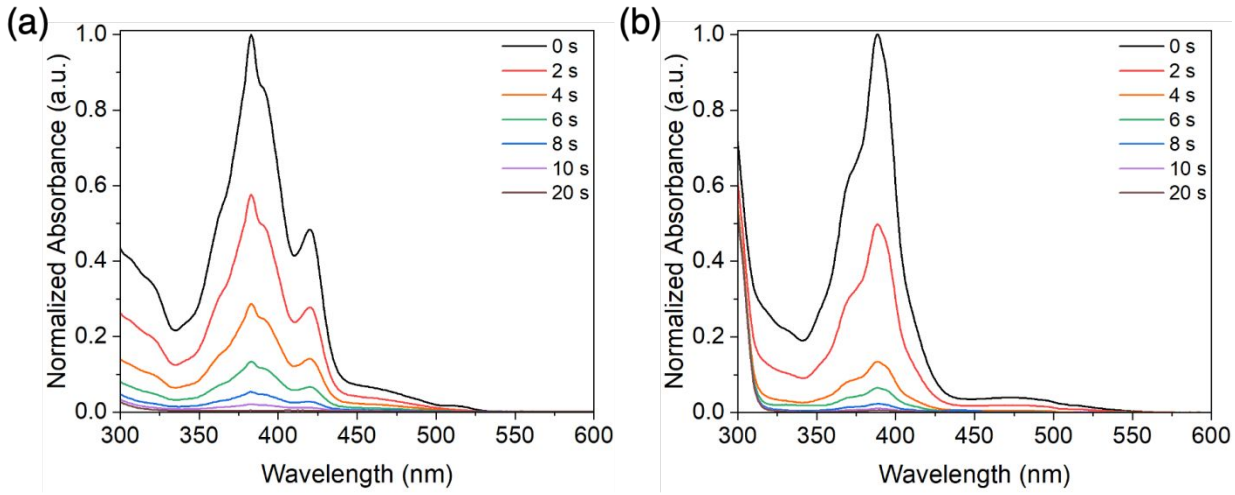

Figure 2. Normalized steady-state absorption spectra of (a) **1** and (b) **2** in chloroform showing the decay in absorbance during continuous photolysis at 365 nm (14 mW/cm^2).

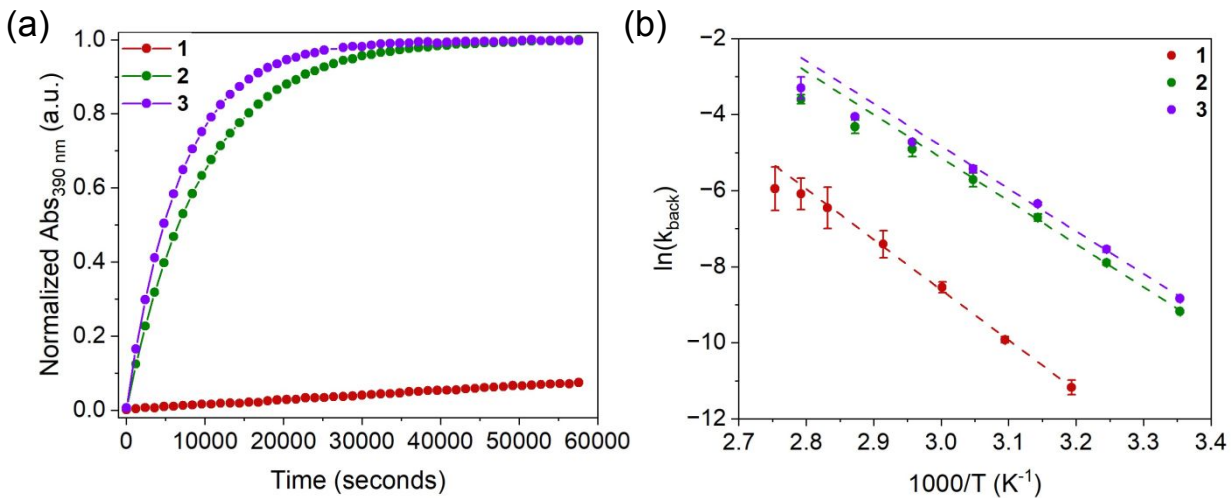

Figure 3. (a) Thermal recovery of **1** – **3** in toluene at 25 ºC, measured over time via UV/vis spectroscopy at 390 nm. (b) Arrhenius plots for the thermal recovery process of **1'** – **3'** in toluene. Experimentally determined activation energy barriers (E_a) and Arrhenius pre-factors (A) are as follows: **1'** (E_a = 110.1 ± 2.5 kJ/mol | A = 3×10^{13}) **2'** (E_a = 94.3 ± 2.0 kJ/mol | A = 4×10^{12}) **3'** (E_a = 93.1 ± 3.2 kJ/mol | A = 3×10^{12}). Values were determined based on the line of best fit that was constructed using data points between 40 – 80 ºC for **1'** and 25 – 55 ºC for **2'** and **3'**.

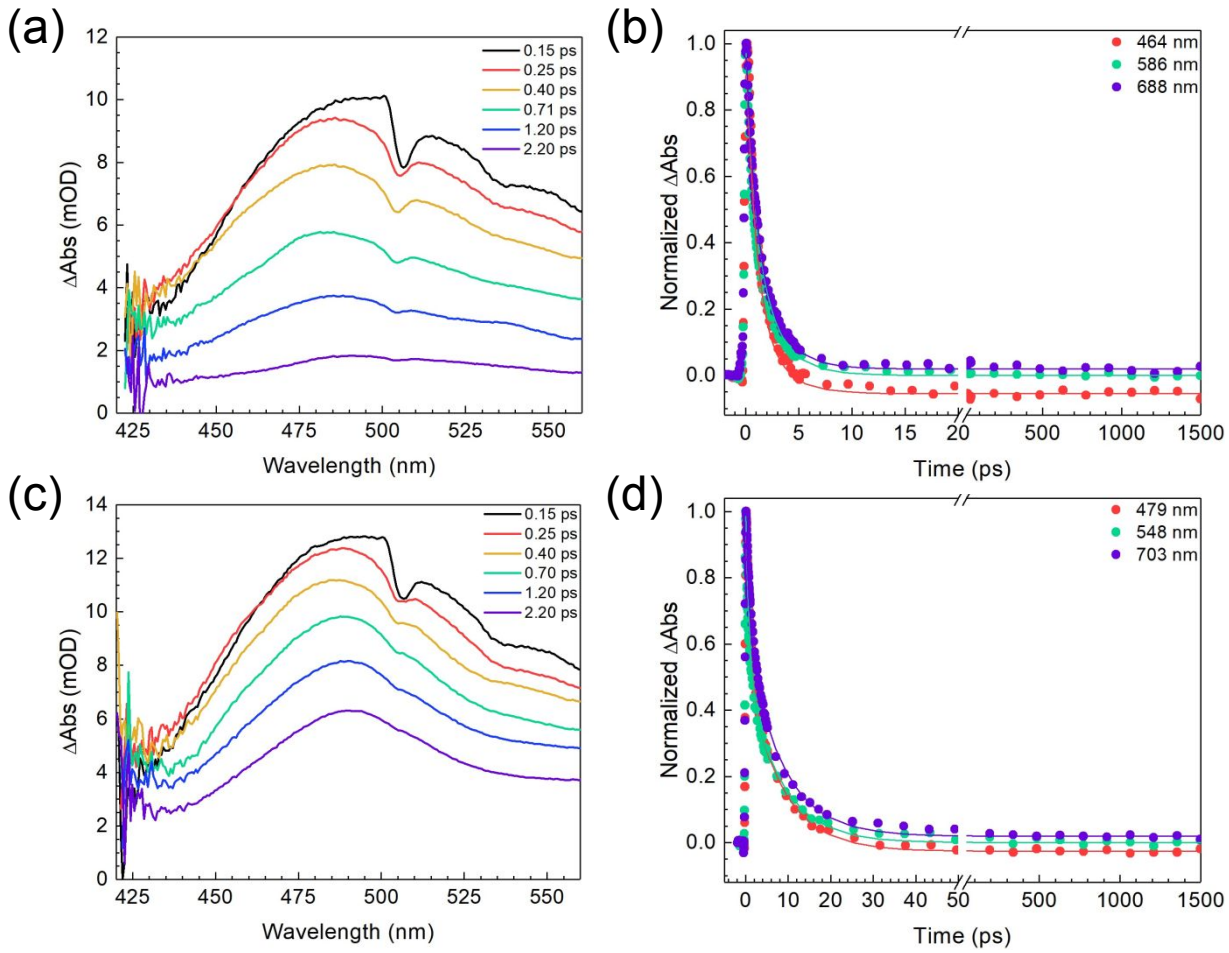

Figure 4. (a) Femtosecond transient absorption measurements of **1** showing the spectral evolution at various delays after the 400 nm beam pump. (b) Fs-TA measurements showing the biexponential decay kinetics of **1.** (c) Fs-TA measurements of **2** showing the spectral evolution at various delays after the 400 nm beam pump. (d) Fs-TA measurements showing the biexponential decay kinetics of **2**.

Table 1. Tabulated time constants (τ) and their respective weighted contributions (A_n) for **1** and **2** from femtosecond transient absorption experiments with photoexcitation (λ_{ex}) at 400 nm and 470 nm. Experiments performed with 400 nm photoexcitation were fit to a biexponential decay, and the 470 nm experiment was fit to a single exponential decay. The wavelengths of the kinetics traces (λ_{obs}) were chosen at the zero-crossing point of any long-lived signal; no offsets (y_0) were needed in fitting.

Molecule	λ_{ex} (nm)	λ_{obs} (nm)	A_1	τ_1 (ps)	A_2	τ_2 (ps)	y_0
1	400	586	0.56	0.5	0.44	2.3	0
2	400	548	0.49	0.7	0.51	8.1	0
2	470	543	-	-	1.00	8.1	0

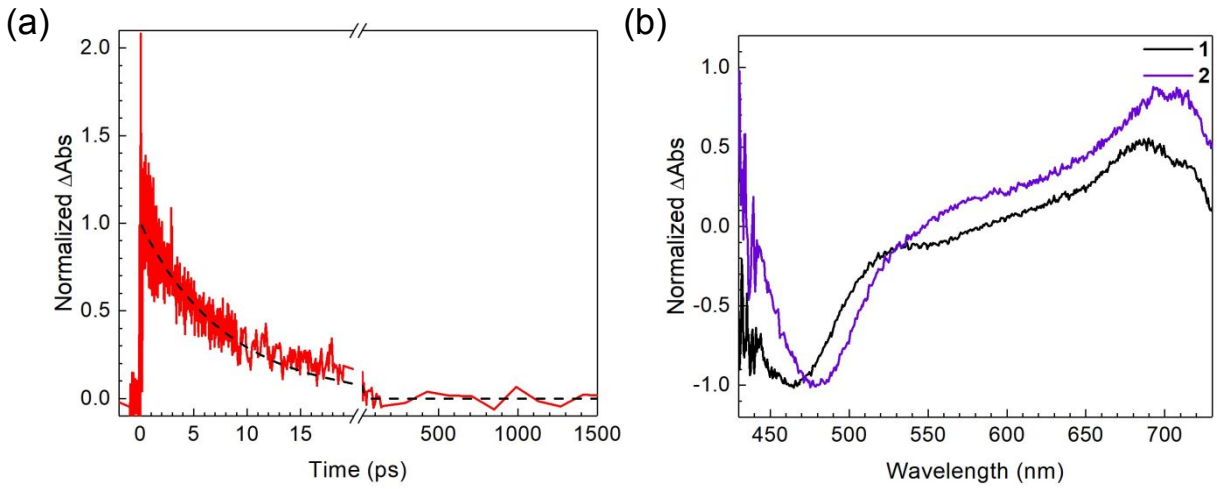

Figure 5. (a) Femtosecond transient absorption measurements showing the single exponential decay kinetics that are present when **2** is pumped at 470 nm. (b) Fs-TA measurements showing the long-time change in absorption features of **1** (black) and **2** (purple) after the 400 nm pump. Kinetics were fit at the zero-crossing point of the long-lived spectra to avoid any contribution of the long-time species on the early-time kinetics. Spectra were averaged across multiple time points, t≥150 ps, to improve signal to noise.

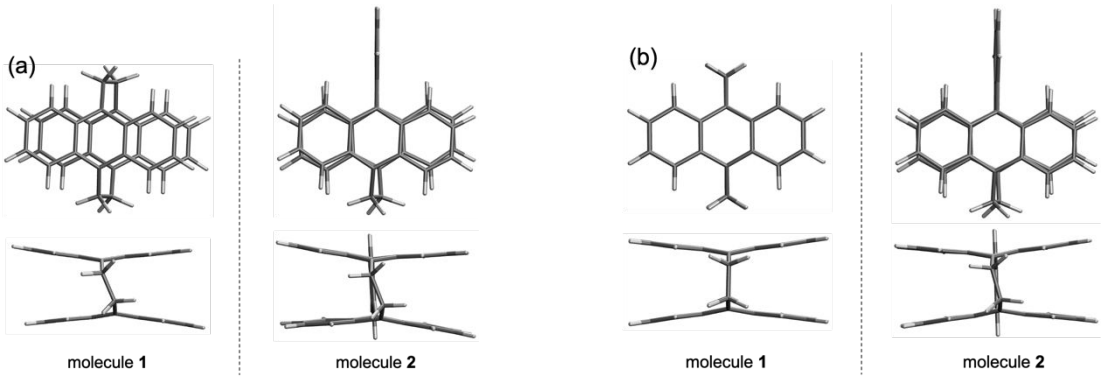

Figure 6. (a) Ground state and (b) S_A state structures of **1** (left) and **2** (right) optimized at the CAM-B3LYP-D3/cc-pVDZ level.

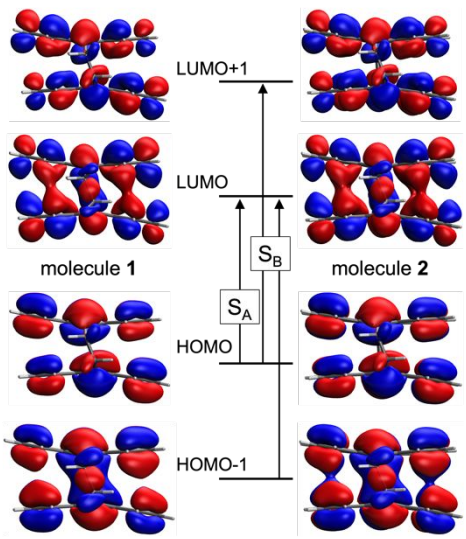

Figure 7. Frontier MOs of **1** (left) and **2** (right) molecules computed at the CAM-B3LYP-D3/cc-pVDZ level. Vertical arrows indicate main contributions to charge-resonance (S_A) and bright (S_B) excited states.

Table 2. Decomposition of electronic transitions to singlet excited states of **1** and **2** (S_0 geometry) in terms of local excitations (within of each anthracene unit, LE_1 and LE_2) and charge transfer (CT_{12} and CT_{21}) computed at the CAM-B3LYP-D3/cc-pVDZ level. Boldface indicates the bright state (S_B) corresponding to the main absorption band of the spectra.

	molecule **1**				molecule **2**			
state	CT_{12}	CT_{21}	LE_1	LE_2	CT_{12}	CT_{21}	LE_1	LE_2
S_1	0.219	0.219	0.248	0.248	0.219	0.219	0.249	0.249
S_2	0.429	0.429	0.019	0.019	0.430	0.430	0.023	0.023
S_3	**0.013**	**0.013**	**0.447**	**0.447**	0.104	0.104	0.364	0.364
S_4	0.092	0.092	0.385	0.385	**0.022**	**0.022**	**0.443**	**0.443**
S_5	0.226	0.226	0.201	0.201	0.061	0.061	0.398	0.398
S_6	0.019	0.019	0.455	0.455	0.183	0.183	0.260	0.260

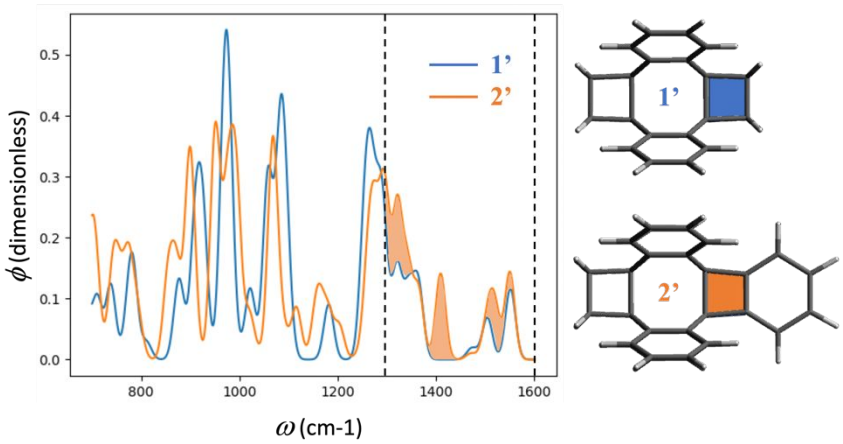

Figure 8. (Left) Ring-deformation function (equation 1) for photodimers **1'** and **2'** computed for a single 4-membered ring (the one fused to the phenyl ring in **2'**). Each $d_{ik}(\omega_k)$ contribution is represented by a gaussian function centered at ω_k with a full width at half maximum of 10 cm^{-1}. Increase of in-plane ring deformation of **2'** with respect to **1'** within the 1300-1600 cm^{-1} region is highlighted in orange. (Right) Molecular models of **1'** and **2'** indicating the 4-membered ring considered (N_R atoms in equation 1).

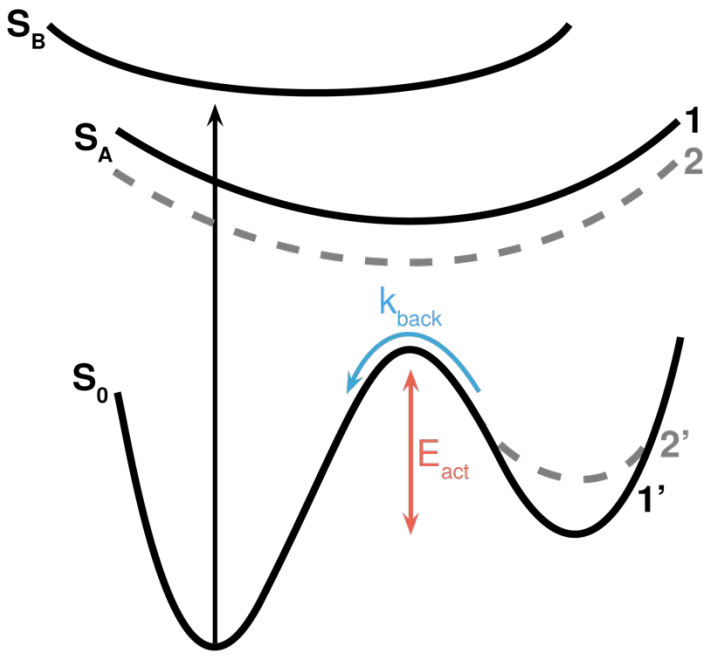

Figure 9. Schematic representation of the different possible pathways available after excitation from the ground state into the S_B state.

The data supporting this article have been included as part of the Supplementary Information